01 Jan 2018

A Constitutive Model for Entangled Polydisperse Linear Flexible Polymers with Entanglement Dynamics and a Configuration Dependent Friction Coefficient. Part II. Modeling "Shear Modification" Following Cessation of Fast Shear Flows

David W. Mead

Saman Monjezi

Joontaek Park
Missouri University of Science and Technology, parkjoon@mst.edu

Recommended Citation

D. W. Mead et al., "A Constitutive Model for Entangled Polydisperse Linear Flexible Polymers with Entanglement Dynamics and a Configuration Dependent Friction Coefficient. Part II. Modeling "Shear Modification" Following Cessation of Fast Shear Flows," *Journal of Rheology*, vol. 62, no. 1, pp. 135-147, American Institute of Physics (AIP), Jan 2018.
The definitive version is available at https://doi.org/10.1122/1.5009187

A constitutive model for entangled polydisperse linear flexible polymers with entanglement dynamics and a configuration dependent friction coefficient. Part II. Modeling "shear mod...

Article *in* Journal of Rheology · January 2018
DOI: 10.1122/1.5009187

3 authors, including:

Saman Monjezi
Missouri University of Science and Technology
12 PUBLICATIONS **67** CITATIONS
SEE PROFILE

Joontaek Park
Missouri University of Science and Technology
33 PUBLICATIONS **100** CITATIONS
SEE PROFILE

A constitutive model for entangled polydisperse linear flexible polymers with entanglement dynamics and a configuration dependent friction coefficient. Part II. Modeling "shear modification" following cessation of fast shear flows

D. W. Mead[a)]

Mead Consulting, Bedford, New Hampshire 03110

S. Monjezi and J. Park[b)]

Chemical and Biochemical Engineering Department, Missouri University of Science and Technology, Rolla, Missouri 65409

(Received 7 April 2017; final revision received 7 August 2017; published 16 November 2017)

Abstract

The polydisperse Mead–Park (MP) "toy" molecular constitutive model developed in Paper I [Mead *et al*., J. Rheol. **62**, 121–134 (2017)] as well as our previously published work [e.g., J. Rheol. **59**, 335–363 (2015)] is used in the "forward" direction to study model polydisperse melts of entangled linear flexible polymers in severe, fast shear flows. The properties of our new model are elucidated by way of numerical simulation of a representative model polydisperse polymer melt in step shear rate and interrupted shear flow. In particular, we demonstrate how the MP model simulates the individual molecular weight distribution (MWD) component dynamics as well as the bulk material properties. Additionally, we demonstrate that the polydisperse MP model predicts the phenomenon of "shear modification" for model MWD's with a long, high molecular weight tail. Specifically, the terminal dynamic moduli following cessation of severe, disentangling deformation, are shown to slowly heal/recover on the orientational relaxation time scale of the longest chains in the MWD. This is the first molecular constitutive equation to predict the phenomenon of shear modification. We provide detailed insight into the molecular mechanism responsible for this previously enigmatic and important phenomenon. Additionally, the presence of shear modification is not necessarily associated with the presence of shear stress peak overshoot transients in interrupted shear flow. Specifically, we examine and analyze the interrupted shear experiments reported by Tsang and Dealy [J. Non-Newtonian Fluid Mech. **9**, 203–222 (1981)] and demonstrate quantitatively their lack of a relationship to shear modification. We also demonstrate that the new MP model accurately predicts the Cox-Merz rule, Laun's rule and Gleissele's mirror relations in steady shear. https://doi.org/10.1122/1.5009187

I. INTRODUCTION

In our previous papers [1,2] and Paper I (Part I of our three companion papers), we developed the Mead–Park (MP) "toy" molecular constitutive model for entangled mono and polydisperse linear flexible polymers that holds forth promise in predicting both extensional and shear flow properties in the highly nonlinear flow regime. In this paper, we continue our study of the MP model by examining model polydisperse systems in fast shearing flows. We shall consider model molecular weight distributions (MWDs) with P discrete weight fractions, $\sum_{j=1}^{P} w_j = 1$. Here and throughout this paper subscripts denote discrete molecular weight components *not* tensor component indices.

We shall choose to test the new polydisperse MP model by modeling rheological phenomena that are thought to be particularly sensitive to the entanglement dynamics such as "shear modification." Shear modification is widely believed to be related to deformation driven disentanglement of the high molecular weight chains and a consequent lowering of the modulus and all rheological properties related to it. Shear modification is a deformation induced reduction in modulus that can persist for hours, or days following cessation of fast deformation in some instances. Shear modification manifests itself in many rheological properties of the melt following severe disentangling deformation. Properties such as the dynamic moduli, $G^*(t,\omega)$, die swell (unconstrained elastic recovery), extensional viscosity and strain hardening, melt flow index (MFI), melt strength and the recoverable compliance are all impacted by severe disentangling deformations [3–5].

It was reported that MFI of linear polyethylene without shear history increases after its being melted and sheared [6]. The changes of viscosity and elasticity of linear polyethylene after capillary extrusion were compared to find that the elasticity recovers with time while the viscosity remains the same, which indicates the recovery of the entanglement microstructure [7]. The viscosity and the elasticity of isotactic polypropylene were found to be dependent on the shear and thermal history [8]. The recovery of the storage modulus after strongly shearing linear polypropylene was measured to find that the rate of recovery is affected more by molecular structure than initial modification [9].

[a)]Electronic mail: meaddavid@hotmail.com
[b)]Author to whom correspondence should be addressed; electronic mail: parkjoon@mst.edu

The phenomenon of shear modification is entirely reversible upon healing/annealing the polymer sample above the melt temperature for hours/days or alternatively, dissolving it in solvent and precipitating it. Both procedures retrieve the equilibrium entanglement microstructure with no chemical change in the molecular architecture or MWD.

In this paper, we shall explicitly consider the case of recovery of the terminal dynamic moduli following cessation of fast, severe steady shear flow, $G^*(t,\omega)$. The linear viscoelastic (LVE) dynamic moduli are a direct physical manifestation of the entanglement microstructure [10,11]. Lower dynamic moduli reflect a lower entanglement density for the time scales being probed. We shall also consider "interrupted shear" experiments which are also thought to be sensitive to the entanglement microstructure. In this case, the rest time between step shear rates, t_{rest}, is thought to partially allow the entanglement microstructure to heal before the subsequent step shear rate is applied [12,13].

In order to make quantitative calculations with the new MP model, we need to identify the molecular model parameters in particular the set of orientational and stretch relaxation times, $\{\tau^0_{d,i}\}$ and $\{\tau^0_{s,i}\}$ as a function of molecular weight. In this manuscript, we use a naïve parameter identification scheme that does *not* account for contour length fluctuations (CLF). The MP model collapses to the Double Reptation model in the LVE limit. A fundamental flaw of the Double Reptation model is that it ignores the effect of CLF and the MP model inherits this defect. We defer until Paper III the complication of determining the molecular MP parameters that do include the impact of CLF the derivation of which is complex and involved [14,15]. Our purpose in this manuscript is to elucidate the fundamental properties of the basic MP model that are not impacted by CLF. In particular, we shall demonstrate that the MP model predicts shear modification as well as the Cox-Merz rule and its derivatives.

This paper is organized in the following manner: We do not present or outline the polydisperse MP model which has been described in Paper I along with our previously published work [1,2,16,17], rather we elucidate some of the unique properties of the model by way of example. Specifically, we shall show that the new model can predict the phenomenon of shear modification in polydisperse linear polymers [5–9]. To this end, Sec. II uses the polydisperse MP model in the forward direction to simulate fast, transient shear flow experiments for model MWD's. Specifically, Sec. II A details the model polystyrene (PS) melt to be studied and how the model parameters are calculated. Section II B predicts the interrupted shear properties of model PS melt systems. With the MP model properties illustrated in the forward direction, in Sec. II C we then proceed to demonstrate that the MP model predicts shear modification for model MWD's with high molecular weight tails following fast, steady shear flow. Section III addresses phenomena in interrupted shear experiments on high density polyethylene (HDPE) melts as reported by Tsang and Dealy [12,13] and their relationship to shear modification. In Sec. IV, we summarize and discuss our results.

II. ILLUSTRATION OF MP MODEL PROPERTIES IN TRANSIENT SHEAR FLOWS FOR MODEL MWD'S OF PS MELTS

In this section, we simulate severe, transient shear flows of model MWD polymer systems using the polydisperse MP model. This allows us to illustrate the properties and capabilities of the model for classic rheometric flows. We are also motivated to illustrate the model properties to subsequently compare and contrast them with experimental data of Tsang and Dealy [12,13] in Sec. III. The example we detail in this section is for a fast, severe shear flow of PS whereas Tsang and Dealy were limited by the onset of edge fracture and hence worked with comparatively slow flow of polyethylene. We will identify features of fast, severe flows of PS such as shear modification that are not present in the comparatively slow flows of polyethylene studied by Tsang and Dealy.

Fast, severe transient shear flow excites both stretch and orientational relaxation modes of linear polymers in a complex manner. Additionally, transient shear flow has orientation angles varying dynamically between 45° for linear flows, and 0° for very fast shear flows thus fully testing the differential description of the orientation dynamics, Eqs. (3) and (4) of Paper I. Hence, transient shear flows present a rigorous, general illustration of all aspects of the polydisperse MP model.

A. Description and characterization of the model polymer melt examined in fast, stretching shear flows

We shall proceed as follows. First, we shall select a model MWD of a typical polymer melt. Specifically, we shall choose a Wesslau log-normal MWD of a PS melt at $T = 170\,^{\circ}\text{C}$. We shall subject this model system to step shear rate and interrupted shear rate experiments and thereby elucidate some of the properties and capabilities of the polydisperse MP model. The weight average molecular weight, M_w, of the PS system is 250 000 Daltons and the polydispersity index for the log-normal MWD is $M_w/M_n = 4$. The MWD is discretized into seven slices for computational speed and ease of interpretation. The discrete MWD is plotted in Fig. 1 and logged in Table I.

To compute the set of stretch and longest relaxation times $\{\tau^0_{d,i}\}$ and $\{\tau^0_{s,i}\}$ we shall assume a universal functional form based on the method described by Pattamaprom and Larson [18–20] and previously employed by Mishler and Mead [16,17]. The longest bare orientational relaxation time, $\tau^0_{d,i}$, for PS, and other linear melts, has the following universal form (see Fig. 2),

$$\tau^o_{d,i}(M_i,T) = \begin{cases} \tau^o_{s,i}(M_i,T) & \text{for} \quad M_i < M_c \\ 2\tau_e(T)\left(\dfrac{M_i}{M_c}\right)^{\alpha} & \text{for} \quad M_i > M_c. \end{cases} \tag{1}$$

Here, the material dependent constants are the "critical" molecular weight for entanglement, M_c, an equilibrium time of entangled segments, $\tau_e(T)$ and the power law exponent, α. The fundamental idea in invoking the above structure is to exploit the near universal structure of the longest relaxation

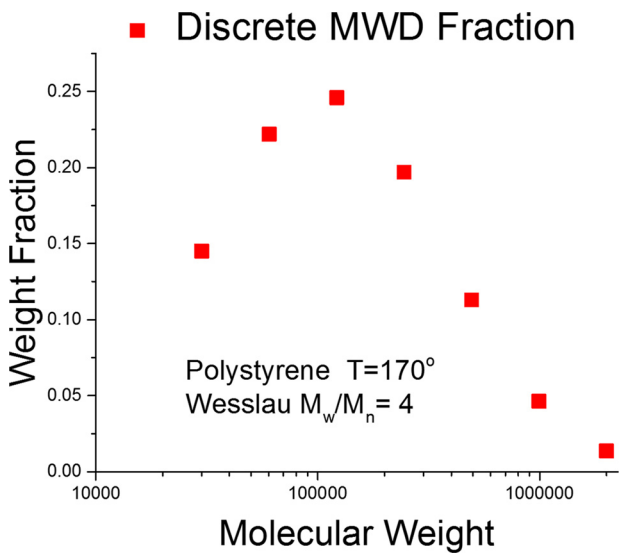

FIG. 1. Plot of the discrete MWD (w_i vs M_i) of the model PS melt studied in Sec. II B. We use a Wesslau log-normal MWD typical of many commercial addition polymers as our model MWD. Only seven discrete MWD fractions were used in the simulation for clarity and simplicity of interpretation.

time of linear polymers as a function of M_i, $\tau_{d,i}(M_i,T) \approx (\eta_o(M_i,T))/G_N^o$, as first demonstrated in the classic work of Berry and Fox [21] (see Fig. 2). For PS melts $\tau_e(170^\circ) = 2.7 \times 10^{-3}$ s [19,22]. Physically, the parameter $\tau_e(T)$ is equal to the Rouse relaxation time at M_c. For PS, $M_c = 26\,000$ and is usually about twice the entanglement molecular weight, M_e. The power law exponent α is ~ 3.4 for PS melts with molecular weights in this range. The above parameter values for PS melts are consistent with other researchers [19,20].

The prefactor of 2 in Eq. (1) appears as a consequence of the double reptation expression for the longest relaxation time in terms of the orientational relaxation time in a hypothetical matrix of fixed obstacles, i.e., orientational relaxation without constraint release effects. Note that for components of the MWD below the critical molecular weight for

TABLE I. Properties of the discrete Wesslau log-normal molecular weight PS melt studied in Sec. III. Only seven discrete slices were used to simplify data mining, presentation and interpretation. The variables in the tables are (from the left to right) the index, the molecular weight, the weight fraction, the longest relaxation time, the stretch relaxation time, the total number of entanglements, the stretch dilution, and the effective stretch relaxation time of each component at equilibrium, respectively (see the Nomenclature of Paper I: "0" indicating equilibrium properties). Note that the stretch tube dilution is significant for all high molecular weight components of the MWD.

i	$M_i \times 10^6$	w_i	$\tau^0_{d,i}$ (s)	$\tau^0_{s,i}$ (s)	N^0_i	Ψ^0_i [a]	$\tau^{eff}_{s,i} = \tau^0_{s,i}/\Psi^0_i$
1	0.0300	0.147	0.0197	0.0197	2.31	1.00	0.0197
2	0.0604	0.226	0.130	0.0799	4.65	0.853	0.0937
3	0.122	0.250	1.40	0.324	9.36	0.627	0.5167
4	0.245	0.200	15.2	1.31	18.8	0.627	2.0893
5	0.493	0.115	164.0	5.33	37.9	0.376	14.176
6	0.993	0.0472	1.77×10^3	21.6	76.4	0.176	122.73
7	2.00	0.0138	1.91×10^4	87.6	154.0	0.176	497.73

[a] $1 - \Psi^0_i$ is the equilibrium "dilution" level of solvent like entanglements with respect to stretch of the long chains defined by the cutoff criteria $\tau^0_{s,i}/\Psi^0_i\tau^0_{d,j} > 1$.

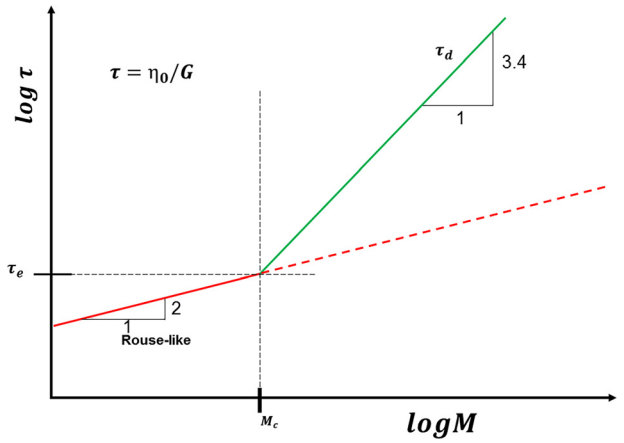

FIG. 2. Sketch of the idealized universal form of the relationship between the bare longest relaxation time, $\tau^0_{d,i}$, the stretch relaxation time $\tau^0_{s,i}$ and molecular weight, M_i, used in this work. The universal model parameters are τ_e, M_c, and α. These three parameters completely specify all the relaxation times for an arbitrary molecular weight in a polydisperse system.

entanglement we are setting the longest orientational relaxation time equal to the Rouse time.

The corresponding monodisperse stretch (Rouse) relaxation times for a PS melt are simply calculated as [20]

$$\tau_{s,i}(M_i,T) = \tau_e(T)\left(\frac{M_i}{M_e}\right)^2. \quad (2)$$

The above parameter identification scheme does *not* include the effects of CLF. In this sense, the parameter identification is naïve and only strictly applies to polymer systems with more than ~30 entanglements, i.e., where CLF's are relatively unimportant compared to reptation. A parameter identification procedure that does include CLF has been previously detailed by Ye *et al.* [14,15] for the polydisperse Mead-Larson-Doi (MLD) model which, like the MP model, also collapses to the Double Reptation model in the LVE limit. We defer establishing a comprehensive and detailed parameter identification scheme until Paper III. This paper is directed at determining the properties of the MP model, such as shear modification, which are independent of the parameter identification scheme used.

B. Simulation of interrupted shear experiments for a model PS system

In this section, we simulate the interrupted shear experiment on the PS melt described in Sec. II A above and thereby illustrate a number of features of the new MP model for polydispersity as well as establish a base case to subsequently study the interrupted shear data of Tsang and Dealy [12,13]. We start with a an interrupted shear protocol comprised of shearing at $10\,s^{-1}$ for 20 s followed by a shear free "rest period" of $t_{rest} = 10$ s and finished off by a restart of shear at $10\,s^{-1}$. Before examining the bulk response of the material, we note with reference to Table II that at a shear rate of $10\,s^{-1}$ we anticipate exciting the stretch modes of the upper half of the MWD, i.e., those MWD components where

TABLE II. Properties of the model polyethylene melt used to simulate the experiments of Tsang and Dealy [12,13]. Note the small 2.5 wt. % high molecular weight "spike" at 1×10^7 Daltons. Only seven discrete slices of the MWD have been taken for simplicity and ease of presentation and interpretation (see Fig. 11).

i	$M_i \times 10^6$	w_i	$\tau^0_{d,i}$ (s)	$\tau^0_{s,i}$ (s)	N^0_i	Ψ^0_i	$\tau^{eff}_{s,i} = \tau_{s,i}/\Psi_i$
1	0.0500	0.343	7.93×10^{-5}	1.75×10^{-6}	50.0	1.00	1.75×10^{-6}
2	0.121	0.305	1.60×10^{-3}	1.75×10^{-6}	121	1.00	1.75×10^{-6}
3	0.292	0.197	3.21×10^{-2}	5.98×10^{-5}	292	1.00	5.98×10^{-5}
4	0.707	0.0922	0.647	3.50×10^{-4}	707	0.657	5.33×10^{-4}
5	1.71	0.0312	13.0	2.05×10^{-3}	1.71×10^3	0.353	5.81×10^{-3}
6	4.14	0.00758	262	0.0120	4.14×10^3	0.353	0.0340
7	10.0	0.0250	5280	0.070	1.00×10^4	0.156	0.449

$\dot{\gamma}\tau_{s,i} > 1$. We believe these fast, severe flow conditions are representative of those in a typical extruder.

Figure 3 shows the shear stress vs time for the interrupted shear experiment described above. The first thing to note is that the peak stress levels exceed the magnitude of the plateau modulus for PS ($G^o_N = 200\,000$ Pa) [23]. This is a clear signature that significant stretch is occurring in the melt [24]. Indeed, Fig. 4 shows the relative stretch of the diluted stretch tube and partially disentangled tube stretch of component 6 vs time indicating clearly that the system is significantly stretching. The stretch in the diluted stretch tube is calculated from Eq. (6) of Paper I and that relative stretch value is fed into the Mishler–Mead stretch [16,17] tube coupling equation (12b) via approximate analytic solution shown in Appendix A of Paper I. Note that if we had used the Auhl *et al*. stretch [25] tube coupling equation (12a) spurious unphysical results are generated. Hence, in all calculations in this manuscript we invoke the Mishler–Mead stretch tube coupling equation (12b).

Figure 3 also illustrates that the peak shear stress is only partially recovered after $t_{rest} = 10$ s to anneal the entanglement microstructure. In Fig. 5, we plot the recovery of peak shear stress as a function of rest time. The peak shear stress is recovered on a time scale of order $O(10^2)$ s which corresponds to the longest stretch relaxation times in the system (see Table I). However, as we shall subsequently demonstrate, recovery of the peak overshoot stress does *not* necessarily signal the end of shear modification for these severe flow conditions.

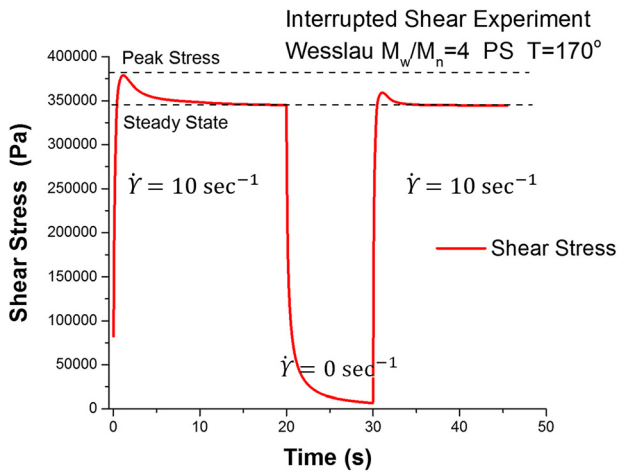

FIG. 3. Plot of the shear stress, σ_{xy}, vs time, t, for the interrupted shear experiment performed on the model PS melt displayed in Fig. 1. Note that the second shear stress overshoot is partially muted by the previous deformation history even though virtually all the shear stress is relaxed during the rest period.

The next bulk figure we examine is the average orientation angle χ vs time, Fig. 6. The average (bulk) orientation angle $\chi(t)$ of a polydisperse system is defined as

$$\chi(t) = \frac{1}{2}\arctan\left[\frac{2\sigma_{xy}(t)}{\sigma_{xx}(t) - \sigma_{yy}(t)}\right] = \frac{1}{2}\arctan\left[\frac{2\sum_i \sigma_{xy,i}(t)}{\sum_i \left(\sigma_{xx,i}(t) - \sigma_{yy,i}(t)\right)}\right], \quad (3)$$

where $\sigma_{xy,i}(t)$, $\sigma_{xx,i}(t)$, and $\sigma_{yy,i}(t)$ are the i MWD component stresses.

The bulk orientation angle displays interesting transients and clearly illustrates that the flow is highly nonlinear since the steady state orientation angle is, $\chi_{ss} \approx 10°$. The χ transients during and after the rest period are associated with the fast, preferential relaxation of the low molecular weight components of the MWD. Specifically, in steady shear flow the orientation of the seven molecular weight components is splayed out like a fan with the low molecular weight components more closely oriented to 45° and the high molecular

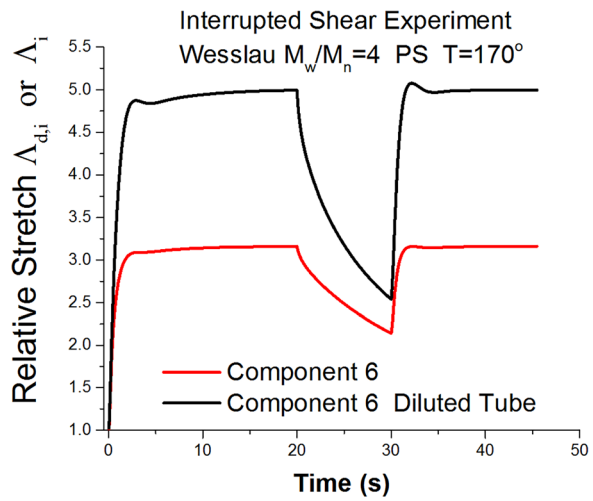

FIG. 4. Plot of the relative stretches of the diluted stretch tube ($\Lambda_{d,I}$ (t): lower line) and the partially disentangled tube (Λ_I (t): upper line) for component 6 in the interrupted shear experiment performed on the model PS melt displayed in Fig. 1. Clearly significant stretch of the high molecular weight components is occurring in shear flow that requires a diluted stretch tube to describe quantitatively.

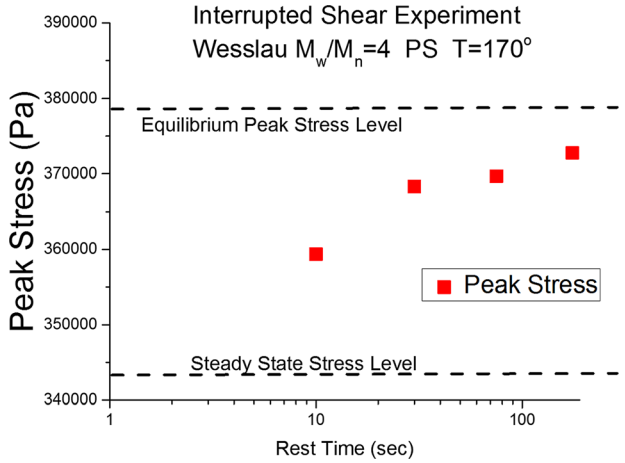

FIG. 5. Plot of the fractional recovery of the peak shear stress, σ_m, as a function of rest time, t_{rest}, for the interrupted shear experiment performed on the model PS melt displayed in Fig. 1. The equilibrium peak stress is completely recovered on time scales of order $O(10^2)$ seconds. This corresponds to the stretch relaxation times of the high molecular weight components of the MWD (see Table I).

weight components more closely aligned in the flow direction, 0° (see Fig. 7). During the rest period, only the high molecular weight highly oriented components are unrelaxed and bear any residual stress which is reflected in the decrease in χ during this period since the relaxed low molecular weight components act effectively as isotropic solvent. Isotropic solvent does not contribute to the optical or stress orientation angle determination. Note that all components of the MWD relax their stress monotonically during the rest period but at very different rates.

Upon resumption of the flow following the rest period the relaxed isotropic components of the MWD are excited and reorient from equilibrium starting at 45° while the partially oriented high molecular weight components do not project significantly onto the velocity gradient resulting in the observed overshoot in χ upon resuming the flow. The distinctive features

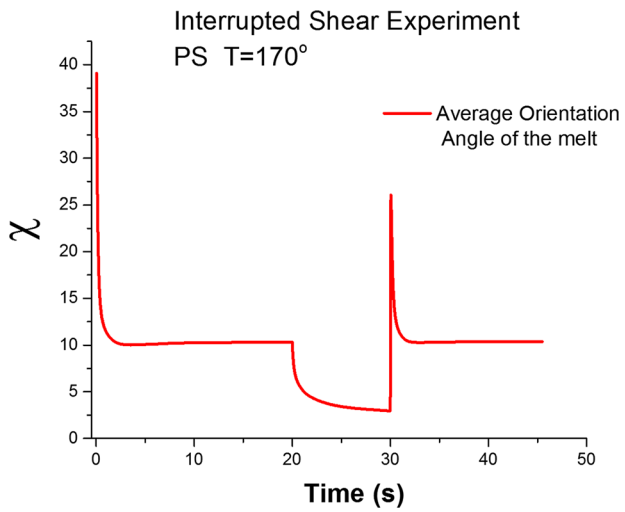

FIG. 6. Plot of the average (bulk) orientation angle, χ, vs time, t, for the interrupted shear experiment performed on the model PS melt displayed in Fig. 1. The flow is highly nonlinear and exhibits distinctive transients associated with differential relaxation/excitation of various components of the MWD [26]. Such behavior can be observed in standard rheo-optical experiments and provides a useful basis for quantitatively evaluating the MP model.

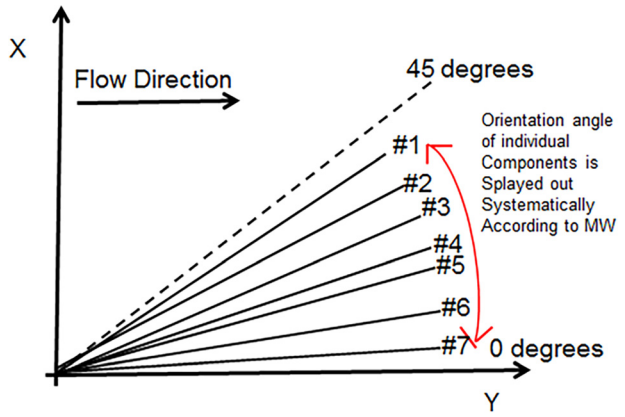

FIG. 7. Qualitative sketch of the steady state orientation angle of each of the seven discrete components in the model PS MWD. In steady state shear, the components splay out and orient systematically according to their molecular weight (relaxation time), i.e., $\chi_i = (1/2)\arctan[2\sigma_{xy,i}/(\sigma_{xx,i} - \sigma_{yy,i})]$. Upon cessation of shear, the fast relaxers effectively "disappear" with respect to their optical contribution to the birefringence leaving only the highly oriented, slow relaxing species to define the bulk orientation angle. This is reflected in a drop in the bulk orientation angle during the rest period. Upon restart of shear the relaxed, isotropic low molecular weight components once again contribute to the bulk orientation angle starting from their linear (equilibrium) value of 45°.

of Fig. 6 provide a useful basis to experimentally evaluate the polydisperse MP model in the future using standard rheo-optical experiments such as those discussed in our previous papers [26,27] where similar interpretations with respect to differential component relaxation have been made.

Continuing to data mine the interrupted shear experiment we next examine the entanglement dynamics of the diluted stretch tube of components 6 and 7 (Table I) in Fig. 8. The first thing to note is that the number of diluted stretch tube entanglements monotonically decreases while the material is being sheared. Since the orientational relaxation times for entanglement recovery [see Eq. (2)] are very large the number of entanglements only slowly recovers during the rest period. It is remarkable to note that the number of entanglements continues to decrease even after hundreds of strain units have been applied to the material. Evidently, Eq. (16) of Paper I only slowly approaches steady state as the material is sheared. This is related to the speed of convection of entanglements off the chain tips, $\underline{\underline{\kappa}} : \underline{\underline{S}}_{tube,i} = \dot{\gamma}\, S_{xy}$, which is typically small in shear flows, relative to the rate of re-entanglement (see Paper I for the variable definitions).

C. Shear modification of model MWD systems of linear polymers following fast shearing flow

In this section, we simulate the phenomenon of shear modification for the model polydisperse PS system described in Sec. II A above. As outlined in the Introduction, shear modification is a deformation induced reduction in modulus that can persist for hours, or days following cessation of deformation in some instances [5–9]. Rheological properties such as the dynamic moduli, $G^*(t, \omega)$ are impacted by severe disentangling deformations [3,4]. Here, the variable t is the rest time following cessation of the severe deformation. The phenomenon is entirely reversible upon healing/annealing the sample above the melt temperature for hours/days or

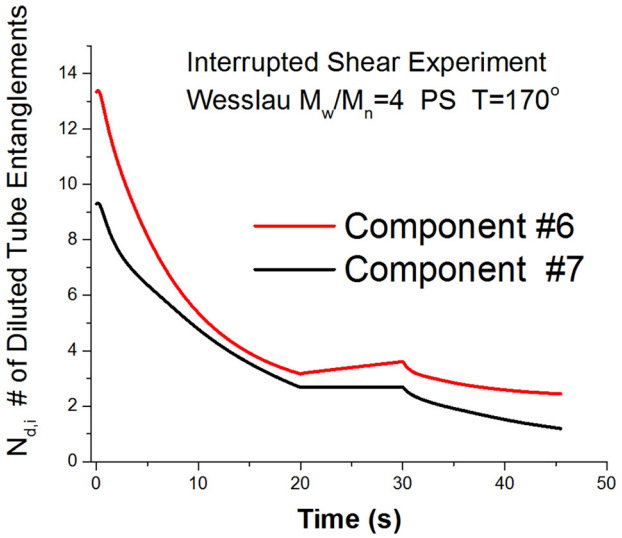

FIG. 8. Plot of the entanglement dynamics in the diluted stretch tube [$N_{d,i}(t)$] for components 6 and 7 for the interrupted shear experiment performed on the model PS melt and conditions displayed in Fig. 1 and described in Table I. Almost 90% of the viable stretch entanglements (i.e., diluted tube entanglements) for each high molecular weight component are annihilated with no indication of abating with further deformation. It takes many hundreds of strain units for Eq. (16) of Paper I to reach its steady state for this polymer system (see Appendix A).

alternatively, dissolving it in solvent and precipitating it. Both procedures are believed to retrieve the equilibrium entanglement microstructure.

We shall explicitly consider the case of recovery of the terminal dynamic moduli following fast, severe steady shear flow, $G^*(t,\omega)$. The LVE dynamic moduli are a direct physical manifestation of the entanglement microstructure [10,11]. Lower dynamic moduli reflect a lower entanglement density for the time scales being probed.

To analyze the flow, we assume that following cessation of deformation the system has relaxed to the extent that the stretch in *all* components is relaxed. For the system described in Sec. II A, Fig. 3 demonstrates that virtually all of the stress has relaxed after ~10 s following cessation of shear. Additionally, we assume that the system is then homogenized such that the average orientation is zero, i.e., nearly isotropic, prior to placing it into the rheometer to measure the LVE properties. In this case, we can approximately calculate the evolution of the LVE material properties in time from stress equation (19) of Paper I as

$$G^*(t,\omega) \approx \sum_i \underbrace{\left(w_i \left(\frac{\sum_k N_{ik}(t)}{N_i^0} \right) G_N^0 \right)}_{i \quad chain\ \text{modulus}} \times \sum_j \underbrace{\frac{N_{ij}(t)}{N_i(t)}}_{\substack{j\ entanglement \\ fraction \\ on\ an\ i\ chain}} \left[\frac{i\omega\tau_{d,ij} + (\omega\tau_{d,ij})^2}{1 + (\omega\tau_{d,ij})^2} \right], \quad (4)$$

where $\tau_{d,ij} = (\tau_{d,i}\tau_{d,j})/(\tau_{d,i} + \tau_{d,j})$ is calculated from Eq. (15) of Paper I in the slow deformation or small strain limit (see Paper I for the variable definitions). Since we have ignored any residual orientation in the system, Eq. (4) constitutes an upper bound on $G^*(t,\omega)$.

Note that for very long times following cessation of steady disentangling deformation the long chain-long chain entanglement microstructure heals via diffusion and, as expected, we retrieve the equilibrium entanglement microstructure result for the dynamic moduli [16,17]

$$\begin{aligned} G^*(t=\infty,\omega) &\approx \sum_i \underbrace{\left(w_i G_N^0\right)}_{\substack{i\ chain \\ modulus}} \sum_j \underbrace{w_j}_{\substack{j\ entanglement \\ fraction}} \left[\frac{i\omega\tau_{d,ij} + (\omega\tau_{d,ij})^2}{1 + (\omega\tau_{d,ij})^2} \right] \\ &= G_N^0 \sum_i \sum_j w_i w_j \left[\frac{i\omega\tau_{d,ij} + (\omega\tau_{d,ij})^2}{1 + (\omega\tau_{d,ij})^2} \right]. \end{aligned} \quad (5)$$

Examining Eq. (4) reveals that there are two separate, but related, effects leading to the lowered dynamic modulus following cessation of fast flows. The first is a lowering of the i-chain modulus/tension by the entanglement dilution factor $\sum_k N_{ik}(t)/N_i^0$. However, this effect is generally smaller and shorter lived in polydisperse systems than the related effect of lowering the j-entanglement fraction on an i-chain by the factor $N_{ij}(t)/N_i(t)$. Lowering the j-entanglement fraction is the principal cause for the prolonged, delayed healing of the terminal dynamic moduli following cessation of severe, disentangling deformation. Physically, lowering the j-entanglement fraction on an i-chain reduces the number of Kuhn bonds associated with the given ij-entanglement pair thereby reducing the associated dynamic moduli. This specifically impacts the long-long entanglement pairs which control the terminal dynamic modulus.

An illustration of these ideas is shown in Fig. 8 where we plot $(N_{ij}(t))/(w_j N_i(t))$ versus t during and after cessation of severe, disentangling deformation illustrated in Fig. 3 for pairs of long–long entanglements. Recall that $N_{ij}(t)/N_i(t)$ represents the fraction of Kuhn bonds on an i-chain oriented by j-entanglements. At equilibrium $N_{ij}(t)/N_i(t)$ is equal to w_j. Hence, $(N_{ij}(t))/(w_j N_i(t))$ represents the departure of the ij entanglement pairs from their equilibrium entanglement microstructure value.

Figures 10(A) and 10(B) show a plot of the storage and loss modulus vs frequency for the same polydisperse material studied in Sec. II B following application of a severe steady shear of 1000 strain units at a shear rate of 10 s^{-1}. This system corresponds to Fig. 9 of Sec. II B with additional severe, steady shear applied. The first thing to observe in Fig. 10(A) is that only the terminal moduli due to the long-long entanglements are impacted by the deformation history. The terminal modulus is severely attenuated by the previous deformation history. This correlates closely with the curve showing the healing of the long-long entanglements $(N_{LL}(t))/(w_L N_L(t))$ where "L" refers to long chains in the MWD in Table I and Fig. 1. Specifically, components 5, 6, and 7 comprise the L components. The modulus slowly recovers as the entanglement microstructure heals to its equilibrium configuration in ~5000 s (O(100) min).

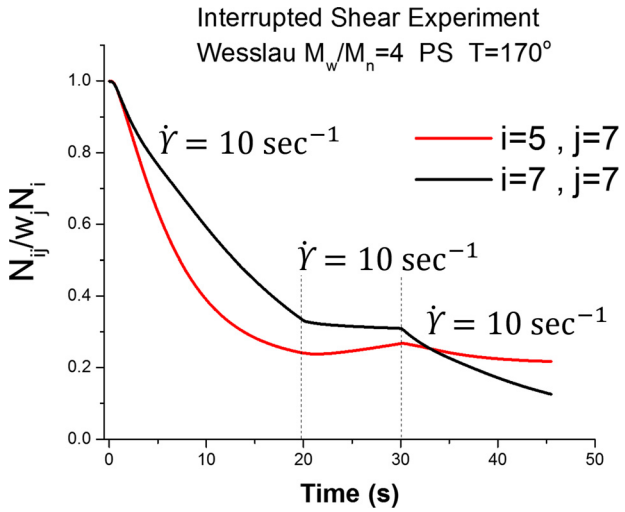

FIG. 9. Plot of $(N_{ij}(t))/(w_jN_i(t))$ vs time for the interrupted shear experiment performed on the model PS melt displayed in Fig. 1. The factor $N_{ij}(t)/N_i(t)$ is divided by w_j to illustrate the departure of the long-long entanglements from their equilibrium entanglement microstructure. Recall that for an equilibrium ij-entanglement microstructure $(N_{ij}(t))/(w_jN_i(t))$ is unity.

This important point is corroborated in Fig. 10 which plots $(N_{ij}(t))/(w_jN_i(t))$ for long-long chain entanglement pairs during and after cessation of shear at $10\,s^{-1}$ for 100 s (1000 strain units!). Here, the dynamics of the individual entanglement pairs can be seen clearly. During shear the fast relaxing entanglement pairs reach a steady state value relatively quickly. Similarly, the fast relaxing pairs recover their equilibrium entanglement density relatively quickly while the slow relaxers languish on time scales of their diffusion driven reorientation. These points can easily be understood by examining Eq. (16) of Paper I in conjunction with the relevant time relaxation time constants in Table I.

The disparate time scales controlling the peak shear stress recovery in the interrupted shear experiment and shear modification experiment suggest that the two phenomena are *not* directly related to one another. We shall probe this point further in Sec. III where we examine interrupted shear data sets for polyethylene from Tsang and Dealy [12,13]. We also developed a method to analytically determine the approximate number of strain units required to induce shear modification (see Appendix A).

III. INTERRUPTED SHEAR FLOW OF TSANG AND DEALY

A phenomenon previously thought to be related to shear modification can be seen experimentally in the interrupted shear experiment [12,13,28,29]. The original idea behind the interrupted shear experiment is that it takes a finite time for the entire entanglement microstructure to heal completely following cessation of fast steady shearing flow. If a step shear rate is initiated prior to complete healing of the entanglement microstructure a different, muted transient response of the material is observed. Previous studies have focused on the peak transient shear stress above the steady state value [12,13], $\sigma_m(t_{rest}, \dot{\gamma})$. These effects are observed for long-

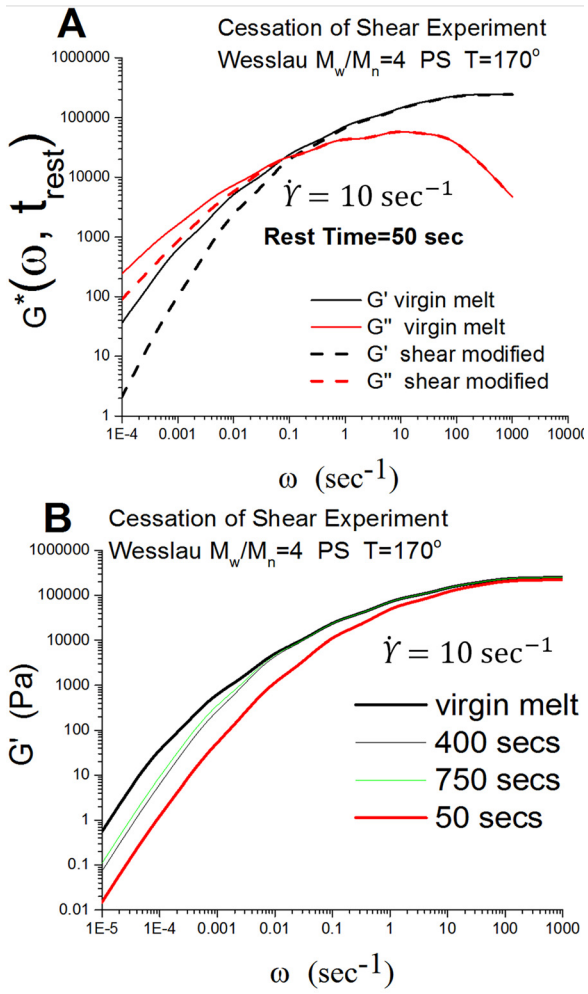

FIG. 10. (A) Plot of the dynamic moduli calculated using Eq. (4) for the virgin PS melt of Fig. 1, Table I and for the shear modified melt 50 s after cessation of steady shear. The melt was "modified" by applying 1000 strain units of $10\,s^{-1}$ shear. Both the storage and loss moduli are significantly diminished by the severe disentangling shear flow. (B) As time elapses the entanglement microstructure slowly heals on a time scale of the long–long entanglements [see Eq. (16) of Paper I] and the equilibrium dynamic moduli are recovered. The dynamic moduli curves for other values of time following cessation for shear are shown to illustrate this point.

chain branching (LCB) polymer melts and linear polymer systems with a long, high molecular weight tail such as HDPE with a log-normal MWD [28,29].

It has been hypothesized by Dealy and Tsang that the interrupted shear flow effect is related to re-entanglement processes, particularly of the high molecular weight species. The molecular model presented in Sec. II provides the means to study in detail the interrupted shear experiment since the entanglement microstructure is known in detail for each component of the MWD. In particular, the orientational relaxation times of the highest molecular weight components in the melt will control the recovery of the long-long chain entanglement microstructure.

With these ideas in mind, we shall approximately simulate the data presented in Dealy and Tsang for the polydisperse linear HDPE resin described in their paper, "Resin 22" [12,13]. In order to proceed to simulate this system, we shall require an approximate MWD and the stretch and longest relaxation times for a PE melt at 170 °C. For the MWD, we

choose a model Wesslau log-normal MWD with $M_w/M_n = M_z/M_w \approx 10$ since Dealy and Tsang report that $M_n = 1.8 \times 10^4$, $M_w = 1.8 \times 10^5$ and $M_z = 1.4 \times 10^6$ for this HDPE resin (see Fig. 11). Additionally, note that we have added a high molecular weight spike of 2.5 wt. % at 1.0×10^7 Daltons to the model MWD. This spike was necessary to improve fits to the rheological data reported by Tsang and Dealy (Fig. 12).

Following the method described in Sec. II A for PS, the longest relaxation time for PE has the same universal form as described in Eqs. (1) and (2) (see Fig. 7). It is appropriate to comment on the order of magnitude of $\tau_e(T)$ for PE at 170°. In particular $\tau_e(T)$ is very small, $\tau_e(170^\circ) \approx O(10^{-9})$. Hence for ordinary commercial molecular weights and ordinary deformation rates at these temperatures it is comparatively difficult to stretch PE even with stretch tube dilution factored in, i.e., $\tau_{s,i}^{eff} = \tau_{s,i}^0/\Psi_i^0$. Compare this to the case studied in Sec. II above. There we did see significant stretch however for PS $\tau_e(170^\circ) \approx O(10^{-3})$. The molecular weights and properties of the model system used to simulate the experiments of Tsang and Dealy is summarized in Table II below.

The first figure we examine is a representative interrupted shear stress vs time plot for the Tsang and Dealy system, Fig. 13. The interrupted shear flow consisted of 60 s of shear at 0.1 s^{-1} followed by a rest time of varying durations. After the rest period, the flow is restarted at the same shear rate and the magnitude of the shear stress overshoot is noted, $\sigma_m(t_{rest}, \dot{\gamma})$.

The first thing to note in Fig. 13 is the magnitude of the shear stresses, O(1) kPa, three orders of magnitude less than the plateau modulus for PE (2.6 MPa) [23]. Hence, we can immediately conclude that there is very little chain stretch of the main MWD components occurring in this system even though the flow is highly nonlinear [24]. This point can be corroborated by referring to the stretch relaxation times in Table II and applying the test $\dot{\gamma}\tau_{s,i} > 1$. The nonlinearity of the flow is demonstrated by the steady state orientation angle corresponding to 0.1 s^{-1}, $\chi \approx 19^\circ$.

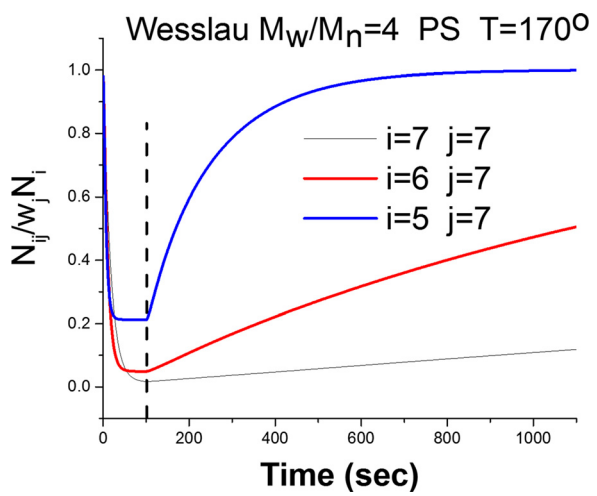

FIG. 11. Plot of $N_{ij}(t)/w_j N_i(t)$ vs time for three long-long entanglement pairs of PS from Fig. 1, Table I during and following the cessation of shear at 10 s^{-1} for a 100 s period. The time scale for the healing of the long-long entanglements [see Eq. (2)] is *identical* to that for the recovery of the shear modified dynamic moduli (Fig. 10). This point can be seen directly from the model for shear modification of the dynamic moduli, Eq. (4).

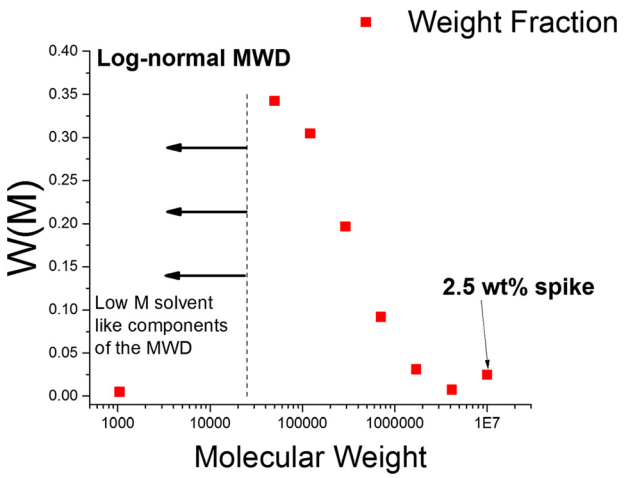

FIG. 12. Plot of the discrete model MWD used to simulate the Tsang and Dealy interrupted shear experiments. Note that a 2.5 wt. % high molecular weight spike has been added to the log-normal model MWD to improve the fit to the rheological data. Additionally, all the low molecular weight species were lumped together into a single low molecular weight fraction. This was done to increase the size of the time step used for computational speed in the numerical integration scheme and does *not* change the rheological predictions for these experiments. In the same context, we have selected only seven slices for the discrete MWD. In principle, we can choose an arbitrary number of slices at the expense of computation time and comprehensibility when data mining the results.

Figure 14 displays the recovery of the peak shear stress transient vs rest time, the function $\sigma_m(t_r, \dot{\gamma})$. Here we see that, unlike the example discussed in Sec. II B, the peak shear stress is recovered on a time scale of the longest orientational relaxation times. Evidently there is more than one means to generate and relax interrupted shear stress peak transients. Additionally, by interrogating the entanglement

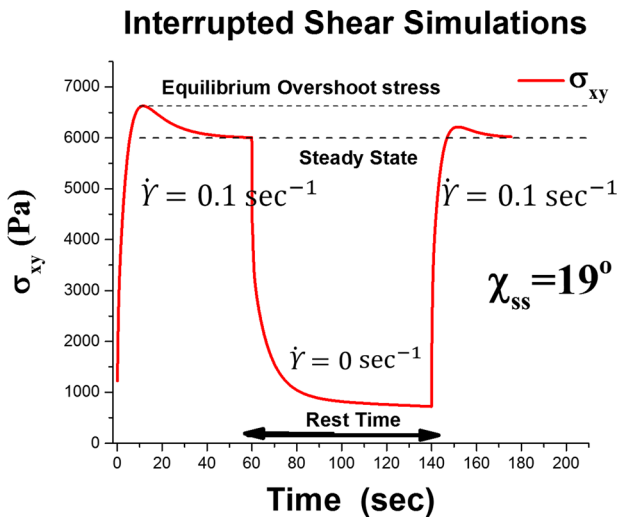

FIG. 13. Plot of the shear stress vs time for the Resin-22 model polyethylene system used to simulate the interrupted shear experiments of Tsang and Dealy [12,13]. Note that the stress levels are of order O(kPa) whereas the plateau modulus for polyethylene is 2.6 MPa. Hence the stress levels are very low and little if any chain stretch is anticipated [24]. Also note that during the rest period shown the stress levels do *not* hit zero. There is still some residual orientation of the very long chains. This residual orientation is what mutes the subsequent overshoot for this system.

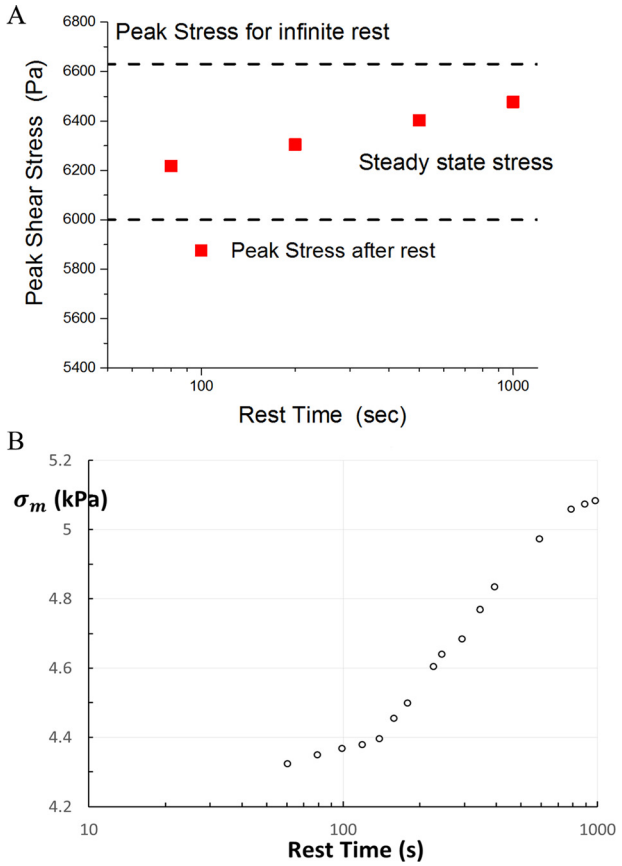

FIG. 14. (A) Plot of the peak stress overshoot, σ_m, vs rest time for the interrupted shear experiment and the Dealy and Tsang model MWD of Fig. 12. The equilibrium peak shear stress is recovered on a time scale of the longest orientational relaxation times of the MWD (see Table II). In Fig. 5 for the model PS system, the peak shear stress was recovered on a time scale of the stretch relaxation times. (B) Experimental data adapted from [12,28].

microstructure we determine that the overall entanglement density remains effectively *constant* at these low shear rates, $0.1\,s^{-1}$. Consequently, there is relatively little shear modification as defined in Sec. II C above, despite the fact that there are significant shear stress peak transients. Hence, in this limit the MP model effectively collapses to the polydisperse MLD model [16,17,30] with a constant entanglement density. We conclude that the experiments of Tsang and Dealy are *not* due to shear modification as defined in this manuscript. Rather, the muted stress overshoots are due to residual orientation of very small amounts of high molecular weight species.

We believe that the following mechanism is responsible for the peak shear stress transients reported by Tsang and Dealy. Following the cessation of deformation only a small fraction of the long-long entanglements remain viable, highly oriented in the flow direction and consequently suppresses the subsequent reorientation of the long chains. The reason for the orientation suppression is that the projection of the oriented long-long entanglements on the velocity gradient is $\dot{\gamma}\, S_{xy}$. However, the long chains are still highly oriented in the flow direction and hence their xy component orientation is $S_{xy} \approx 0$.

Hence even though the shear stress contribution of the long-long entanglements is negligible, the impact on the interrupted shear experiment is profound. This is in large measure a consequence of the diluted stretch tube mechanism for stretching the long chains in a polydisperse matrix that is largely relaxed. Understanding the detailed entanglement microstructure is imperative to properly interpret the interrupted shear experiment.

We can discern yet more detailed information about this flow system from the MP model. The MP model can be interrogated to reveal that all activated high molecular weight species contribute *equally* to the bulk stress while the low molecular weight species act effectively as solvent [30]. Specifically, the dimensionless parameter $\sigma_{xy,i}/(w_i\sigma_{xy,bulk})$ is a measure of the fractional weight based contribution to the bulk stress of the i-component. For exaggerated component contributions to the shear stress $\sigma_{xy,i}/(w_i\sigma_{xy,bulk}) > 1$. The activated high molecular weight components in Fig. 13 all have $\sigma_{xy,i}/(w_i\sigma_{xy,bulk}) \approx 11$! Consequently, by following the dynamics of the long chains alone we can understand the Tsang and Dealy experiments in detail since these activated components totally dominate the rheological response.

Finally, in Figs. 15 and 16 we examine properties of the MP model in steady shear flow. Specifically, in Fig. 15 we display the calculated steady shear viscosity versus shear rate for Resin 22 and compare it with calculated predictions from the Cox-Merz rule and Gleissele's mirror relation [28,31]. Only the nonlinear portion of the flow curve is shown since the Cox-Merz rule is an identity at low shear rates [30]. Clearly, the MP polydispersity model is in quantitative agreement with both the Cox-Merz rule and Gleissele's mirror relation as it must be to be a viable constitutive relation for polydisperse linear polymer melts. Note that the MP model extends the validity of the Cox-Merz rule relative to the MLD model into the flow regime where significant stretch is anticipated in shear flow [30].

Similarly, Fig. 16 shows the calculated predictions of the steady first normal stress coefficient versus shear rate for Resin-22 using the MP model. Also shown are predictions of

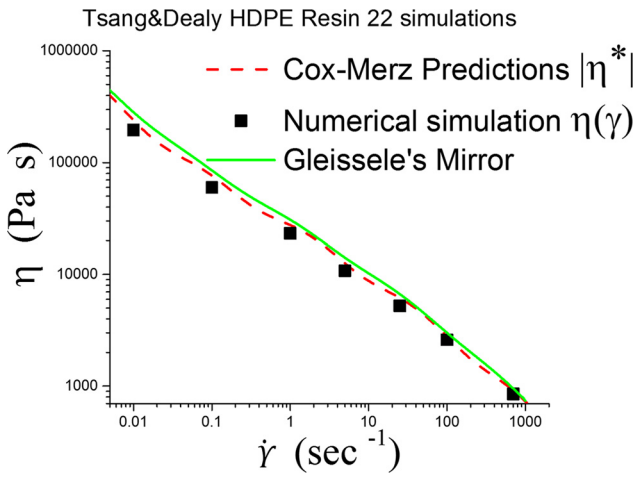

FIG. 15. Plot of the steady state viscosity vs shear rate for the Tsang and Dealy model system Resin-22 shown in Fig. 12. Also shown are the predictions of the Cox-Merz rule and Gleissele's mirror relations. Clearly, the new polydispersity model adheres closely to these well-established empirical relations. Only the nonlinear portion of the flow curve is simulated since the Cox-Merz rule is an identity at low shear rates.

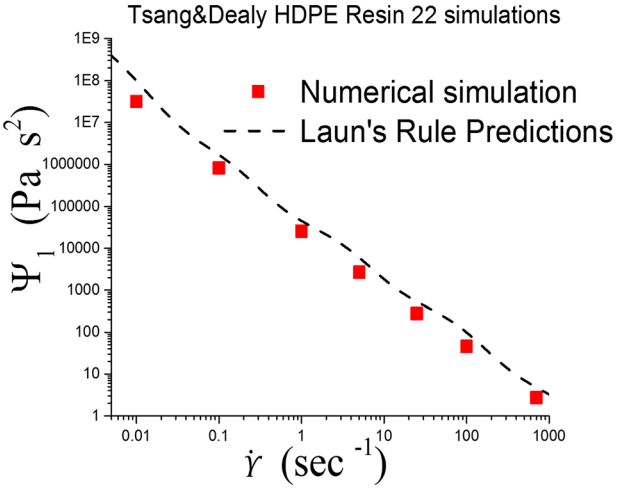

FIG. 16. Plot of the steady state first normal stress coefficient vs shear rate for the Tsang and Dealy model system (Resin-22) shown in Fig. 12. Also shown are the predictions of Laun's rule. Clearly, the new polydispersity model adheres closely to this well-established empirical relationship.

the first normal stress coefficient using Laun's rule [28,31]. Although the predictions from Laun's rule are slightly higher uniformly they are still in good agreement with the calculated values from the MP model. The agreement of the MP model with Laun's rule, the Cox-Merz rule and Gleissele's mirror relation strongly supports the general viability of the polydisperse MP model.

IV. DISCUSSION AND SUMMARY

It has long been known that a polymer melt's rheological properties reflect the underlying fluid microstructure. Microstructure here refers to the MWD, entanglement density and long chain branching [10,11]. Consequently, rheology is commonly used in industry to characterize polymer resins using relatively crude rheological criteria such as the MFI [28,32,33]. Such rheological criteria were until recently largely based on empiricism rather than sound molecular theory. However, molecular rheology has advanced to the point where it is now possible to definitively and quantitatively characterize commercial polymer resins from their rheology alone. These ideas form the motivation and basis of "analytic rheology" as a science.

The ideas and molecular model presented in this paper will allow the science of Analytic Rheology to be extended to include the *nonlinear* viscoelastic material properties whereas in the past only the LVE material properties were used [34]. Analytic Rheology to determine the MWD using nonlinear material functions, such as transient extensional viscosities, has never been attempted let alone accomplished. Transient uniaxial extension will be of particular interest in our subsequent work because of their proven ability to experimentally determine the stretch relaxation spectrum [25]. There are several inherent advantages in nonlinear analytic rheology relative to linear analytic rheology. The conceptual advantages of nonlinear analytic rheology are qualitatively illustrated in Fig. 17.

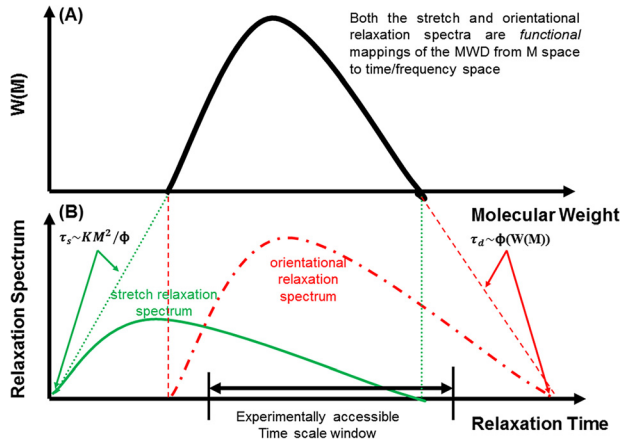

FIG. 17. Sketch of a typical broad MWD for a commercial polymer system with orientational and stretch relaxation spectra overlap. The experimentally accessible time scale window is superimposed on the relaxation time scale axis. For many commercial polymer systems, the longest orientational relaxation times lie beyond the longest experimentally accessible time scale. With respect to Analytic Rheology, both the stretch and orientational relaxation spectra are functionals of the MWD. Note that the high molecular weight tail of the MWD maps into the experimentally accessible time scale window for the stretch relaxation spectrum but not the orientational relaxation spectrum. It is this effect we wish to exploit in our nonlinear analytic rheology inversion scheme. Thus, there are both experimental and theoretical reasons for turning to nonlinear analytic rheology to determine the underlying MWD.

The principal reason why we have chosen to simulate and emphasize shear modification experiments for broadly polydisperse system with our new molecular model of polydispersity is to distinguish the MP model from other models for polydispersity. For example, none of the MLD family of models [16,17,35–37], or the Graham-Likhtman-McLeish-Milner (GLaMM) family of models [38–40], can possibly simulate shear modification experiments. The reason for this is that both families of polydispersity models assume a *constant* entanglement density. We believe that a detailed description of the entanglement dynamics is necessary to understand shear modification. Our very simple description of the entanglement dynamics is one example of the type of molecular model required to capture the phenomenon of shear modification.

We have demonstrated that shear modification is an important feature of the rheology of polydisperse linear polymers. We now argue that shear modification is a *dominant* feature of polydisperse systems with LCB such as low density polyethylene [3,4]. For polymer systems with LCB $\tau^1_{d,i}(t)$ in Eq. (16) of Paper I will explode in magnitude such that shear modification will occur at even the most trivial deformation rates and subsequently take an exorbitant amount of time to heal (days). Indeed, this is what is observed experimentally [3,4]. Despite this fact, theoretically shear modification, and the entanglement dynamics required to describe it, have been absent from nonlinear molecular models for systems with LCB such as the "pom-pom" family of constitutive equations [41]. The pom-pom model and its relatives all assume a *constant* entanglement density which is reflected in the fact that the equilibrium plateau modulus scales the stress.

The key to understanding the shear modification experiments is following the entanglement dynamics of the long chains in the MWD. Experimentally, uniaxial extension is

known to yield the highest degree of shear modification [3]. This can be understood by examining Eq. (16) of Paper I which describes the entanglement dynamics. When the convection term $\underline{\underline{\kappa}} : \underline{\underline{S}}_{tube,i}$ is large, entanglements will be stripped off the chains at a faster rate in uniaxial extensional flow relative to shearing flows which have a smaller projection of the velocity gradient onto the orientation tensor.

Although shear modification may seem a subtle feature of the rheology of polymer melts it can have profound effects on crystallization mechanisms in commercially important polymers such as polyethylene and polypropylene [42–44]. In particular, polymer melt crystallization mechanisms are significantly impacted by long chain-long chain entanglements [45] which we have demonstrated to be severely impacted by fast flows. These flows lead to disentanglement and highly extended conformations (see Fig. 4 in Paper I [46]) which directly impact the crystallization kinetics and morphology as well as the rheology. Only models with entanglement dynamics can predict highly extended chain conformations. Neither the MLD family or GLaMM family of molecular models can predict the development of such entities after many hundreds of strain units of deformation because they have an assumed constant entanglement density.

ACKNOWLEDGMENTS

D.W.M. acknowledges the use of the computational facilities at the City College of New York. S.M. and J.P. acknowledge financial support from the Missouri University of Science and Technology.

NOMENCLATURE

In this Glossary, we list all the terms and their definitions for quick reference. Please also see the Glossary of Paper I for the terms defined in Paper I.

τ_e	an equilibrium time of a single entangled segment
M_c	critical molecular weight for entanglement
α	power law exponent for equation (1)
t_{rest}	the time interval for the shear free rest period
$\chi(t)$	average bulk orientation angle
χ_{ss}	steady state average bulk orientation angle
σ_m	the peak transient shear stress after a rest
λ_{ij}	asymptotic time constant
N_{ij}^{ss}	the number of ij pair entanglement at steady state
T*	the characteristic time scale to achieve a steady state after startup of shear flow
γ^{ss}	the amount of extensional strain to achieve steady state

APPENDIX A: ANALYSIS TO DETERMINE THE APPROXIMATE NUMBER OF STRAIN UNITS REQUIRED TO INDUCE SHEAR MODIFICATION

In this Appendix, we analytically calculate the approximate number of strain units that need to be applied to achieve steady state entanglement dynamics. Since entanglement dynamics control shear modification this is equivalent to determining the number of strain units required to shear modify a melt at a prescribed shear rate. Our analysis begins with the ED equation (16) of Paper I,

$$\dot{N}_{ij}(t) = \frac{N_{ij}^0 - N_{ij}(t)}{\tau_{d,i}^1(t)} - \beta\left[\underline{\underline{\kappa}} : \underline{\underline{S}}_{tube,i} - \frac{\dot{\Lambda}_i(t)}{\Lambda_i} + \frac{\dot{\alpha}_i(t)}{\alpha_i(t)}\right] \times N_{ij}(t) + \frac{N_{ij}^0 - N_{ij}(t)}{\tau_{d,j}^1(t)}. \tag{A1}$$

In order to proceed, we shall have to make some simplifying approximations. Specifically, we shall assume that all transient effects in the entanglement convection term of Eq. (A1) are negligible. Initially, we shall consider shear flow and subsequently generalize the analysis to consider extensional flow. With these assumptions and restrictions, Eq. (A1) simplifies to

$$\dot{N}_{ij}(t) \approx \frac{N_{ij}^0 - N_{ij}(t)}{\lambda_{ij}} - \beta\dot{\gamma}S_{xy}N_{ij}(t), \tag{A2}$$

where $\lambda_{ij} \equiv (\tau_{d,i}^1(t)\tau_{d,j}^1(t))/(\tau_{d,i}^1(t) + \tau_{d,j}^1(t)) \approx (\tau_{d,i}\tau_{d,j})/(\tau_{d,i} + \tau_{d,j})$ and the steady state xy orientation is S_{xy}. (Note that λ_{ij} is a time constant in this Appendix and *not* the relative stretch.) We have suppressed the complex time dependence of λ_{ij} such that it is approximately constant and equal to the reduced diffusive reptation time of the ij pair. With this assumption Eq. (A2) is a first order ordinary linear differential equation. The steady state solution N_{ij}^{ss} can be determined by inspection as

$$N_{ij}^{ss} \approx \frac{N_{ij}^0}{1 + \beta S_{xy}\dot{\gamma}\lambda_{ij}}. \tag{A3}$$

Note that $N_{ij}^{ss} \to 0$ smoothly as $\dot{\gamma}\lambda_{ij} \to \infty$.

The general solution to Eq. (A2) can be also be written immediately as

$$N_{ij}(t) = N_{ij}^{ss}\left[1 - \exp\left\{-t\left(\frac{1}{\lambda_{ij}} + \beta\dot{\gamma}S_{xy}\right)\right\}\right] = N_{ij}^{ss}\left[1 - \exp\left\{-\frac{t}{T^*}\right\}\right]. \tag{A4}$$

The characteristic time scale T* to achieve a steady state after startup of shear flow is therefore

$$T^* = \frac{\lambda_{ij}}{1 + \beta S_{xy}\dot{\gamma}\lambda_{ij}}. \tag{A5}$$

We now have enough information to address the question of how many strain units are required to achieve shear modification. Recall that $\beta \approx 0.12$ and $S_{xy} \approx 0.15$ for fast shear flows. Hence, $\beta S_{xy} \approx O(10^{-2})$ for shear flows. For fast flows, the high molecular weight ij component pairs will generally satisfy $\dot{\gamma}\lambda_{ij} \gg 100$ and hence, $T^* \approx 100/\dot{\gamma}$. The corresponding shear strain required to achieve steady state is therefore $\gamma_{ss} = T^*\dot{\gamma} \approx 100$. Hence it will take at least 100 shear strain units to shear modify a melt for marginal cases such as that

of Tsang and Dealy. We can also calculate $N_{77}^{ss}/N_{77}^{0} \approx 0.91$ from Eq. (A3) for the worst case ij entanglement pair scenario for the Tsang and Dealy Resin-22. This approximate calculation is in line with what we calculate rigorously with our computer program. Hence we should not expect shear modification for Resin-22 which is precisely what we calculated.

Note that the onset of shear modification is controlled by the magnitude of the ij entanglement pair orientation time and *not* the stretch relaxation time. We now repeat the above analysis for the case of extensional flow and demonstrate that extensional flows are much more efficient at generating shear modification. For fast extensional flows, $\underline{\underline{\kappa}} : \underline{\underline{S}}_{tube,i} \approx \dot{\varepsilon}$. The analysis for extensional flows is identical except that $\dot{\gamma} S_{xy}$ is replaced by $\dot{\varepsilon}$. Hence, $\mathrm{T}^{*} = \lambda_{ij}/(1 + \beta \dot{\varepsilon} \lambda_{ij}) \approx 10/\dot{\varepsilon}$ for $\dot{\varepsilon}\lambda_{ij} \gg 10$ and the characteristic time T$*$ is reduced by an order of magnitude. Similarly, the amount of extensional strain is greatly reduced to $\gamma_{ss} = \mathrm{T}^{*}\dot{\varepsilon} \approx 10$. This brief analysis demonstrates what is observed experimentally, i.e., that extensional flows are much more efficient at generating shear modification than shear flow.

References

[1] Mead, D. W., N. Banerjee, and J. Park, "A constitutive model for entangled polymers incorporating binary entanglement pair dynamics and a configuration dependent friction coefficient," J. Rheol. **59**, 335–363 (2015).

[2] Park, J., D. W. Mead, and M. M. Denn, "Stochastic simulation of entangled polymeric liquids in fast flows: Microstructure modification," J. Rheol. **56**, 1057–1081 (2012).

[3] Rokudai, M., "Influence of shearing history on the rheological properties and processability of branched polymers. I," J. Appl. Polym. Sci. **23**, 463–471 (1979).

[4] Leblans, P., and C. Bastiaansen, "Shear modification of low-density polyethylene: Its origin and its effect on the basic rheological functions of the melt," Macromolecules **22**, 3312–3317 (1989).

[5] Teh, J., A. Rudin, and H. Schreiber, "Shear modification of a linear low density polyethylene," J. Appl. Polym. Sci. **30**, 1345–1357 (1985).

[6] Heitmiller, R., R. Naar, and H. Zabusky, "Effect of homogeneity on viscosity in capillary extrusion of polyethylene," J. Appl. Polym. Sci. **8**, 873–880 (1964).

[7] Schreiber, H., A. Rudin, and E. Bagley, "Separation of elastic and viscous effects in polymer melt extrusion," J. Appl. Polym. Sci. **9**, 887–892 (1965).

[8] Schertzer, R., A. Rudin, and H. P. Schreiber, "Shear and thermal history effects in polypropylene melts," J. Appl. Polym. Sci. **31**, 809–821 (1986).

[9] Breuer, G., and A. Schausberger, "Recovery of shear modification of polypropylene melts," Rheol. Acta **50**, 461–468 (2011).

[10] Andreev, M., R. N. Khaliullin, R. J. Steenbakkers, and J. D. Schieber, "Approximations of the discrete slip-link model and their effect on nonlinear rheology predictions," J. Rheol. **57**, 535–557 (2013).

[11] Schieber, J. D., and M. Andreev, "Entangled polymer dynamics in equilibrium and flow modeled through slip links," Annu. Rev. Chem. Biomol. Eng. **5**, 367–381 (2014).

[12] Dealy, J., and W. K. Tsang, "Structural time dependency in the rheological behavior of molten polymers," J. Appl. Polym. Sci. **26**, 1149–1158 (1981).

[13] Tsang, W.-W., and J. Dealy, "The use of large transient deformations to evaluate rheological models for molten polymers," J. Non-Newtonian Fluid Mech. **9**, 203–222 (1981).

[14] Ye, X., R. G. Larson, C. Pattamaprom, and T. Sridhar, "Extensional properties of mono and bidisperse polystyrene solutions," J. Rheol. **47**, 443–468 (2003).

[15] Ye, X., and T. Sridhar, "Effects of the polydispersity on Rheological properties of entangled polystyrene solutions," Macromolecules **38**, 3442–3449 (2005).

[16] Mishler, S., and D. Mead, "Application of the MLD 'toy' model to extensional flows of broadly polydisperse linear polymers: Part I–Model development," J. Non-Newtonian Fluid Mech. **197**, 61–79 (2013).

[17] Mishler, S., and D. Mead, "Application of the MLD "toy" model to extensional flows of broadly polydisperse linear polymers: Part II. Comparison with experimental data," J. Non-Newtonian Fluid Mech. **197**, 80–90 (2013).

[18] Menezes, E., and W. Graessley, "Nonlinear rheological behavior of polymer systems for several shear-flow histories," J. Polym. Sci. Part B Polym. Phys. Ed. **20**, 1817–1833 (1982).

[19] Pattamaprom, C., and R. G. Larson, "Predicting the linear viscoelastic properties of monodisperse and polydisperse polystyrenes and polyethylenes," Rheol. Acta **40**, 516–532 (2001).

[20] van Meerveld, J., "A method to extract the monomer friction coefficient from the linear viscoelastic behavior of linear, entangled polymer melts," Rheol. Acta **43**, 615–623 (2004).

[21] Berry, G. C., and T. G. Fox, "The viscosity of polymers and their concentrated solutions," in *Fortschritte der Hochpolymeren-Forschung* (Springer, Berlin, 1968).

[22] Arnett, R. L., and C. P. Thomas, "Zero-shear viscosity of some ethyl branched paraffinic model polymers," J. Phys. Chem. **84**, 649–652 (1980).

[23] Fetters, L. J., D. J. Lohse, D. Richter, T. A. Witten, and A. Zirkel, "Connection between polymer molecular weight, density, chain dimensions, and melt viscoelastic properties," Macromolecules **27**, 4639–4647 (1994).

[24] Mead, D. W., D. Yavich, and L. G. Leal, "The reptation model with segmental stretch," Rheol. Acta **34**, 360–383 (1995).

[25] Auhl, D., P. Chambon, T. C. McLeish, and D. J. Read, "Elongational flow of blends of long and short polymers: Effective stretch relaxation time," Phys. Rev. Lett. **103**, 136001 (2009).

[26] Mead, D., and R. Larson, "Rheooptical study of isotropic solutions of stiff polymers," Macromolecules **23**, 2524–2533 (1990).

[27] Oberhauser, J. P., L. Leal, and D. W. Mead, "On the response of entangled polymer solutions to step changes in shear rate: Signatures of segmental stretch?," J. Polym. Sci. Part B Polym. Phys. Ed. **36**, 265–280 (1998).

[28] Dealy, J. M., and K. F. Wissbrun, *Melt Rheology and its Role in Plastics Processing* (Van Nostrand Reinhold, New York, 1990).

[29] Stratton, R. A., and A. F. Butcher, "Stress relaxation upon cessation of steady flow and the overshoot effect of polymer solutions," J. Polym. Sci. Part B Polym. Phys. Ed. **11**, 1747–1758 (1973).

[30] Mead, D. W., "Analytic derivation of the Cox–Merz rule using the MLD 'toy' model for polydisperse linear polymers," Rheol. Acta **50**, 837–866 (2011).

[31] Bird, R. B., R. C. Armstrong, and O. Hassager, *Dynamics of Polymeric Liquids. Vol. 1: Fluid Mechanics* (Wiley Interscience, New York, 1987).

[32] Dealy, J. M., and R. G. Larson, *Structure and Rheology of Molten Polymers* (Hanser, Munich, 2006), pp. 30–39.

[33] Dealy, J. M., and P. C. Saucier, *Rheology in Plastics Quality Control* (Hanser Publishers, Munich, 2000).

[34] Mead, D., "Determination of molecular weight distributions of linear flexible polymers from linear viscoelastic material functions," J. Rheol. **38**, 1797–1827 (1994).

[35] Mead, D., R. Larson, and M. Doi, "A molecular theory for fast flows of entangled polymers," Macromolecules **31**, 7895–7914 (1998).

[36] Mead, D., "Development of the 'binary interaction' theory for entangled polydisperse linear polymers," Rheol. Acta **46**, 369–395 (2007).

[37] Mead, D., "Derivation of the 'switch function' in the Mead–Larson–Doi theory," Rheol. Acta **50**, 631–643 (2011).

[38] Likhtman, A. E., and R. S. Graham, "Simple constitutive equation for linear polymer melts derived from molecular theory: Rolie–Poly equation," J. Non-Newtonian Fluid Mech. **114**, 1–12 (2003).

[39] Graham, R. S., A. E. Likhtman, T. C. McLeish, and S. T. Milner, "Microscopic theory of linear, entangled polymer chains under rapid deformation including chain stretch and convective constraint release," J. Rheol. **47**, 1171–1200 (2003).

[40] Read, D., K. Jagannathan, S. Sukumaran, and D. Auhl, "A full-chain constitutive model for bidisperse blends of linear polymers," J. Rheol. **56**, 823–873 (2012).

[41] McLeish, T., and R. Larson, "Molecular constitutive equations for a class of branched polymers: The pom-pom polymer," J. Rheol. **42**, 81–110 (1998).

[42] Yamazaki, S., F. Gu, K. Watanabe, K. Okada, A. Toda, and M. Hikosaka, "Two-step formation of entanglement from disentangled polymer melt detected by using nucleation rate," Polymer **47**, 6422–6428 (2006).

[43] Eder, G., H. Janeschitz-Kriegl, and S. Liedauer, "Crystallization processes in quiescent and moving polymer melts under heat transfer conditions," Prog. Polym. Sci. **15**, 629–714 (1990).

[44] Graham, R. S., "Molecular modelling of flow-induced crystallisation in polymers," J. Eng. Math. **71**, 237–251 (2011).

[45] Seki, M., D. W. Thurman, J. P. Oberhauser, and J. A. Kornfield, "Shear-mediated crystallization of isotactic polypropylene: The role of long chain−long chain overlap," Macromolecules **35**, 2583–2594 (2002).

[46] Mead, D. W., S. Monjezi, and J. Park, "A constitutive model for entangled polydisperse linear flexible polymers with entanglement dynamics and a configuration dependent friction coefficient. Part I. Modeling "shear modification" following cessation of fast shear flows," J. Rheol. **62**, 121–134 (2017).